ON THE UNSTEADY AERODYNAMICS OF ROAD VEHICLES IN THE DYNAMIC MOTIONS

S.Y. Cheng[1,5], M. Tsubokura[1], Y. Okada[2], T. Nakashima[3], T. Nouzawa[2], and T. Kobayashi[4]

[1]Hokkaido University, Japan
[2]Mazda Motor Corporation, Japan
[3]Hiroshima University, Japan
[4]Japan Automobile Research Institute, Japan
[5]Universiti Teknikal Malaysia Melaka, malaysia

mtsubo@eng.hokudai.ac.jp

Abstract

Unsteady aerodynamics of road vehicles in dynamic pitching motion were investigated by numerical analysis. Dynamic coupling simulation of flow and vehicle motion was realized based on a large eddy simulation (LES) technique with moving boundary methods. Fully unstructured finite volume code previously developed was implemented for the road vehicle aerodynamics. Arbitrary Lagrangean-Eulerian (ALE) method was employed to handle vehicle's rotating motion, particularly the dynamic pitching. This vehicle motion type is chosen because of the unsteady aerodynamics are expected to be crucial in regards to the comfort of passenger. By using the numerical simulation, a method to estimate the vehicle's aerodynamic damping was proposed.

1 Introduction

Conventionally, the aerodynamic performance of road vehicles has mainly been assessed on the basis of their drag coefficient C_d, which is obtained through steady-state wind tunnel measurements. Thus, it is not adequate to reflect a vehicle's performance with respect to unsteady aspects that are commonly encountered in real life. To consider the stability factors, several assessment methods have been proposed in the literature (e.g. Okada et al, 2009; Howell and Le Good, 1999; Aschwanden et al, 2006). But these methods rely on drive test or wind tunnel measurement, which provide only limited flow information. This can impede detailed flow analysis needed for understanding the underlying mechanism.

A more generalized approach that can be used to assess the aerodynamic stability performance of vehicle under transient situation is highly desirable. Therefore, the present study aims to develop a computational method which can simulate the desired test environment and vehicle motion, for evaluations of vehicle's aerodynamic performance. The method will enable direct comparison of vehicle's stability performance. In addition, the details of flow information that can be obtained with the present numerical method will also enable comprehensive study of the physical mechanism that govern the aerodynamic stability of vehicle.

2 Mathematical formulation

The governing equations adopted in this study are given by the spatially filtered continuity and Navier-Stokes equations for incompressible Newtonian flow, which are expressed in tensor notation as

$$\frac{\partial \overline{u}_i}{\partial x_i} = 0, \tag{1}$$

$$\frac{\partial \overline{u}_i}{\partial t} + \frac{\partial \overline{u}_i \overline{u}_j}{\partial x_j} = -\frac{\partial \overline{P}}{\partial x_i} + 2\frac{\partial}{\partial x_j}(\nu + \nu_{sgs})\overline{S}_{ij} = 0, \tag{2}$$

where the over-bar denotes the spatially filtered quantity, and u_i, ν, and ρ are the *i*-th velocity component, kinetic viscosity, and fluid density, respectively. The strain rate tensor and the filtered pressure in eq. (2) are

$$\overline{S}_{ij} = \frac{1}{2}\left(\frac{\partial \overline{u}_j}{\partial x_i} + \frac{\partial \overline{u}_i}{\partial x_j}\right), \tag{3}$$

$$\overline{P} = \overline{p}/\rho + (\overline{u_i u_j} - \overline{u}_i \overline{u}_j)/3. \tag{4}$$

The effect of subgrid-scale (SGS) turbulence on the grid-scale turbulence motion is represented by the SGS eddy viscosity, which is modeled by Smagorinsky (1963) as

$$\nu_{sgs} = \{C_s g(l^+)\Delta^{1/3}\}^2 \sqrt{2\overline{S}_{ij}\overline{S}_{ij}}, \tag{5}$$

where Δ is the volume of the generic numerical element. The model coefficient C_s is given as 0.15, which is typically used in simulations of flow around a rectangular cylinder. The eddy viscosity is damped in the vicinity of a solid wall using a Van-Driest function:

$$g(l^+) = 1 - \exp\frac{-l^+}{25}, \tag{6}$$

where l^+ is the distance from the wall in wall coordinates.

The governing equations were discretized in space using a vertex-centered unstructured finite volume

method. The second-order central differences were applied for the spatial derivative, blended with the first-order upwind scheme for the convective term in the Navier-Stokes equations to avoid excessive numerical oscillation appearing at coarse tetrahedral elements. It should be noted that the dissipation property of upwind schemes is desirable to a certain extent for engineering applications of the LES on unstructured meshes. As a compromise, the contribution of the upwind discretization to the convective fluxes was set to be as low as 5%. The diffusive fluxes on the volume surface were treated based on the deferred correction formula suggested by Muzaferija (1994) to avoid a checker-board type oscillation. The monotone upwind scheme for conservation laws (MUSCL) by van Leer (1977) was also adopted for the convective term at the region away from the vehicle where upwind dissipation does not affect the wake or near-wall turbulence of the target vehicle.

The time marching was based on the fractional step method by Kim and Moin (1985), in which the 3rd-order Adams-Moulton scheme or the implicit Euler scheme was adopted for the velocity prediction step. The coupling of the velocity and pressure fields to obtain the pressure and to correct the velocity was based on the simplified marker and cell (SMAC) method by Amsden and Harlow (1970). The flow rate on the control-volume surface was estimated following the method proposed by Rhie and Chow (1983) to keep the checker-board type pressure oscillation off. The pressure Poisson equation was solved using the incomplete Cholesky conjugate gradient (ICCG) method.

We used the ALE method (Hirt et al, 1974) to recreate the vehicle's pitching motion during flow simulation. In this method, numerical grids move arbitrarily to capture a vehicle's pitching motion without changing the nodes' topological connectivity. Figure 1 shows the computational domain and grid allocation around the vehicle model. The computational domain comprises of prism and tetrahedral cells. Overall, the whole domain encompasses around 12 million elements with three million nodes.

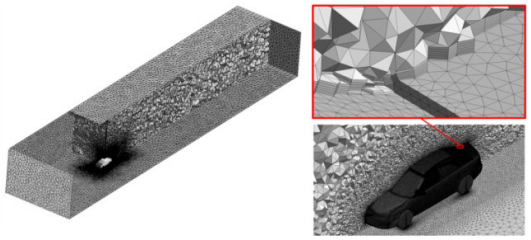

Figure 1: Computational domain (left) and prism mesh layers on vehicle surface (right).

A constant velocity of 39m/s is imposed at the inlet while a simple gradient-free boundary condition is imposed at the outlet. The ground surface was divided into two regions in which free-slip wall boundary was imposed to the $5.0L$ from the inlet to simulate the suction floor effect which prevent the development of boundary layer, while the remaining ground surface was treated by the wall-model assuming a fully developed turbulent boundary layer. Meanwhile, the ceiling and lateral boundaries of the domain were also treated as free-slip wall boundary.

For the given inlet velocity, the airflow Reynolds number with respect to vehicle length is 1.21×10^7. At this high Reynolds number range, it is impossible to allocate sufficient grid resolution at the vehicle surface to resolve the wall boundary layer. Thereby, a universal velocity profile of fully developed turbulent boundary layer is assumed on the vehicle surface. In the assumed velocity boundary, the fluid velocity at the first nearest grid point from the wall is supposed to fit the universal logarithmic law of the mean velocity, and the surface friction is estimated. Then, the obtained surface friction is imposed as a Neumann-type boundary condition of the velocity on the first nearest control-volume surface. To implement this, we employed two strategies to ensure that the resulting y^+ of the first nearest grid point is within the log-law region. First, we created the prism mesh layers at the vehicle surface which enable us to control the normal distance of the first grid point (i.e. 1 mm). Second, we reduced the Reynolds number by one order of magnitude (by decreasing the dynamic viscosity of the fluid). As a result, the y^+ around the vehicle surface is below 30, which enable us to resolve the boundary layer above the buffer layer region.

3 Software and Hardware

The computational code adopted in the present study was originally developed in the "Frontier Simulation Software for Industrial Science" project. The project started in 2002 as an IT research program sponsored by the Ministry of Education, Culture, Sport, Science and Technology of Japan. The authors intensively optimized the code for LES applications under the subsequent IT project "Revolutionary Simulation Software (RSS21)", and parallel and vector efficiency as high as 96% and 99%, respectively, were achieved in simulations performed on 100 nodes/800 CPU. This allowed completion of LES calculations of flow around a formula car with complex geometry in about 120 hours (Tsubokura et al, 2007). The code was then optimized for unsteady vehicle aerodynamics simulations (Tsubokura et al, 2009) under a project supported by an Industrial Technology Research Grant Program in 2007 from the New Energy and Industrial Technology Development Organization (NEDO) of Japan. We are now improving this code for the very large-scale simulation of up to some billion numerical elements to be executed on "K," the world's fastest supercomputer, in Japan.

The present simulation was conducted on the SR11000 supercomputer developed by Hitachi. A total of 16 nodes (256 CPU) was used. It took about 12 hours in wall-clock-time to simulate 1 sec of vehicle motion and the flow around it.

4 Validation

The numerical method was validated in the steady state under the condition that the vehicles were fixed on the floor without any motion. The vehicles used in the validation are simplified sedan-type vehicles with differences in the A-pillar, side skirt, and underbody configurations (see Figure 2). Table 1 summarizes the C_d and C_l measured in the Mazda full-scale wind tunnel and obtained by the present numerical simulation. It should be noted that comparison of the absolute values of C_d and C_l between the wind tunnel data and numerical simulation is only for reference, because the numerical models shown in Figure 2 are the simplified representations of the real vehicle used in wind tunnel measurement (i.e. they are not entirely identical).

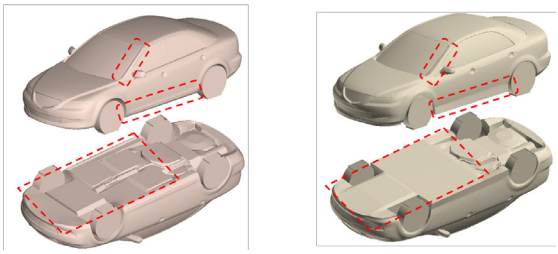

Figure 2: Vehicle models used in validation: Original vehicle (left) and modified vehicle (right).

Table 1 shows that the LES has successfully captured the C_d and C_l improvement tendency in the modified vehicle. In particular, the ΔC_d of numerical simulation is in excellent agreement with the experiment. Whereas a slightly larger discrepancy is identified in ΔC_l, it is still acceptable because the qualitative improvement is well reproduced. Hence, we can deduce that the geometrical differences between these two models are well reproduced numerically.

Table 1: Comparison of C_d and C_l between wind-tunnel measurements and present LES.

	C_d		C_l	
Vehicle	Exp.	LES	Exp.	LES
Original	0.32	0.323	0.20	0.207
Modified	0.30	0.301	0.16	0.142
Difference	-0.02	-0.022	-0.04	-0.065

Figure 3 compares the total pressure distribution behind the side mirror observed in the wind tunnel with that predicted by the present simulation. The typical flow structures around this region are the interaction of two eddies generated by the A-pillar and the side mirror, which are observed on the planes at x=2.26 to 2.86 m in the figure. The simulation results show good agreement with the wind-tunnel measurements.

Figure 4 shows vortex structures extracted from the LES results (left) by expressing the streamlines and velocity magnitude above the trunk deck, and their comparison with the postulated flow structures obtained with wind-tunnel visualization (Okada et al, 2009). The important flow structures above the trunk deck are the two couples of eddies coming from the A and C pillars. In our previous studies on pitching stability, we found that the interactions of these two kinds of eddies profoundly contribute to the aerodynamic damping mechanisms of a vehicle's pitching motion. We can observe that our present simulation generates the expected flow structures above the vehicle. These results clearly indicate that our simulation properly reproduced the difference in flow structures between Vehicle-A and Modified Vehicle-A generated by the slight geometrical differences shown in Figure 2. Based on these simulation results and an intensive comparison of them with the full-scale wind-tunnel measurements, we can say that our simulation is sufficiently correct to discuss the vehicle's aerodynamic stability during pitching.

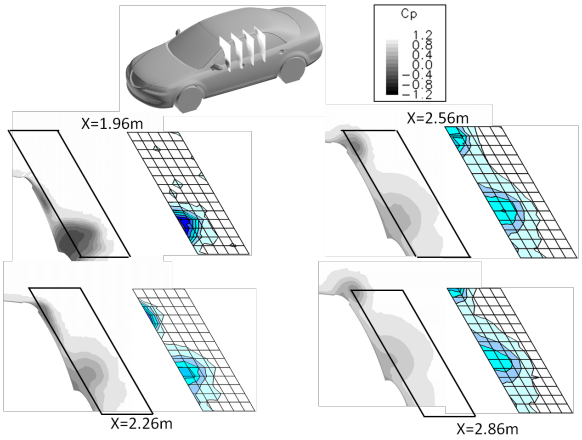

Figure 3: Total pressure distributions around A-pillar and side mirror of Vehicle-A: left, simulation; right, wind-tunnel. The location of each plane is measured from the front end of the vehicle.

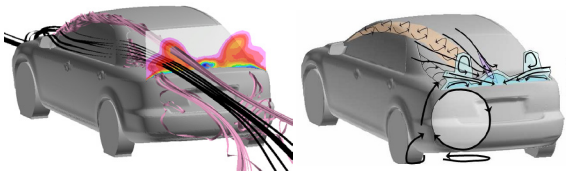

Figure 4: vortex structures of Vehicle-A: Simulation (left) and schematics suggested by wind-tunnel measurements (after Okada et al, 2009) (right).

5 Periodic pitching oscillation

To probe the stability attitude of the vehicles, a periodic pitching oscillation was imposed on them during LES by employing the ALE method. The pitching axis is located at the front-wheel axle. Hence, the models were rotated in a manner that simulates the rear-ride height (RRH) fluctuation of the real vehicles. This corresponds to the fact that the sedan-type vehicles were mainly suffered from RRH fluctuation during road test (Okada et al, 2009). The pitch angle θ of the models is defined as

$$\theta = \theta_0 + \theta_1 Cos\varphi(t), \quad \varphi(t) = 2\pi f_p t \qquad (7)$$

,

By setting θ_0 and θ_1 equal to 0.9, the vehicle models were forced to oscillate at amplitude of 0.9°. The frequency f_p was 1 Hz, which corresponds to Strouhal number (St) of 0.13, normalized by L and inlet flow. This value was chosen in consideration of the road test's RRH fluctuation St of 0.15 obtained by Okada et al (2009).

6 Aerodynamic damping coefficient

To assess the dynamic responses of the models under the influence of pitching oscillation, we decomposed the phase-averaged M into the steady and unsteady components. The equation for phase-averaged M in terms of θ is given as the following expansion,

$$M = C_0 + C_1\theta + C_2\dot{\theta} + C_3\ddot{\theta} \qquad (8)$$

where, respectively, the single dot and double dots in the third and fourth terms indicate the first and second derivatives with respect to θ. Both C_0 and C_1 are static components; the former denotes the pitching moment at zero pitch, while the latter describes the quasi-static behavior by taking into account the pitch-angle variation in a static manner. C_2 is associated with aerodynamic damping, and C_3 is an added moment of inertia that is proportional to angular acceleration.

Substituting Equation (7) into (8) and introducing new coefficients gives

$$M = C_{\text{stat}} + C_{\text{ang}} \sin\phi(t) + C_{\text{dis}} \cos\phi(t) \qquad (9)$$

In Equation (9), the C_{stat} is a constant, and C_{dis} is in-phase with the imposed displacement. In the case of periodic pitching oscillation, these two components produce zero net work on the model over a full cycle of oscillation. On the contrary, C_{ang} which is in-phase with the angular velocity produces work on the model. Hence, this parameter reflects the dynamic response of the vehicle. It depends on the sign of C_{ang}, a negative value implies a tendency for aerodynamics to damp the pitching oscillation, whereas a positive value enhances it. The coefficient thus enables quantitative evaluation of vehicle stability.

7 Comparison of two aerodynamic configurations

On the basis of wind tunnel visualization and road test results, Okada et al (2009) reports that the type of flow structures formed above the truck deck strongly affect the pitching stability attitude of sedan-type vehicle. And the characteristic of the flow structures are depends on the geometrical configurations of the A- and C-pillars. However, the limited flow information that can be obtained through experimental fluid dynamic study impedes comprehensive analysis of the mechanism involved. Therefore, we employed the LES method, which can resolve the details of spatial and temporal information of the flow, to further confirm the findings and investigate the mechanism of aerodynamic damping.

The general geometrical features of the models employed at this stage are based on the original vehicle (Figure 2) but with a flat underbody configuration. We modified the A- and C-pillar configurations to obtain two vehicle models which conform with the characteristic geometry of the stable and less stable sedans reported in our previous investigation. The models are at full scale with similar height H, width W, and length L measurements of 4.7, 2.0, and 1.6m, respectively. The model that represents the vehicle with higher pitching stability has a rounded A-pillar and angular C-pillar configurations, while the one with lower stability adopted the opposite configurations, see Figure 5. The slant angles of the A- and C-pillar of the models are 30° and 25°, respectively. In order for convenient in the discussions, the model represents the vehicle of lower pitching stability is designated "model A", while the other model is termed "model B", hereafter.

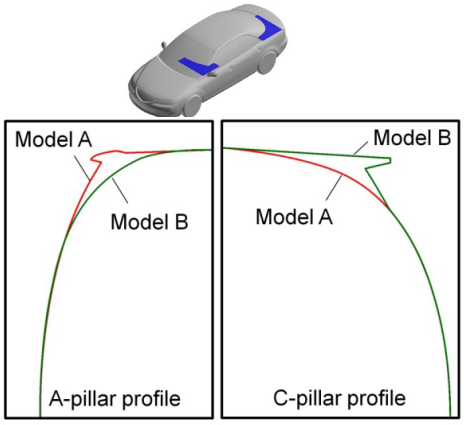

Figure 5: A- and C-pillar configurations.

The C_{ang} of the two models are obtained by fitting their respective phase-averaged M using the nonlinear least squares regression. Figure 6 shows the curves of phase-averaged M and the corresponding fitted functions. The shapes of the curves are similar, but there is a phase shift between them. As a result, model B has a higher negative C_{ang} than model A, by about 20.5%. The higher C_{ang} obtained with model B indicates that its aerodynamic forces induce a higher resisting force on its body motion - stabilizing behaviors. This finding is consistent with the fact that model B was created with aerodynamic features of the real vehicle with higher stability.

Table 2 summarizes the proportional contributions of each vehicle-body part (see Figure 7) on aerodynamic-damping. On average, the underbody has the highest contribution (up to 87.0 and 74.6% in model A and model B, respectively). This result is not surprising because the underbody has the largest surface area and moment arm. However, the main factor that causes the different pitching stability characteristic is the trunk-deck contributions. As presented, the trunk deck contribution in model A is destabilizing, while the one in model B is stabilizing. This opposite tendency agrees to the road test results by Okada et al

(2009) on the basis that the aerodynamic force had acted on the trunk deck of vehicle with lower stability to promote its pitching motion. While in the higher stability vehicle, the aerodynamic force induced a restraining effect.

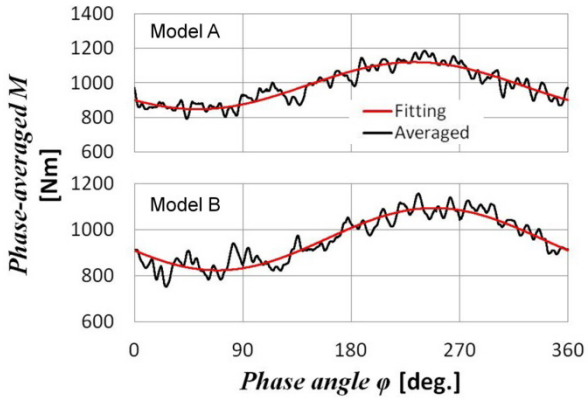

Figure 6: Phase-averaged M and fitted functions.

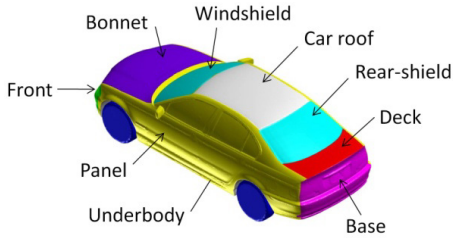

Figure 7: Body-part designations.

Table 2: Contribution of body part on C_{ang}.

C_{ang}	Model A	Model B	diff.	%
Underbody	-92.28	-97.26	-5.0	20.5
Panel	-6.60	-9.73	-3.1	12.9
Car roof	-7.39	-8.50	-1.1	4.6
Windshield	-6.89	-6.26	0.6	-2.6
Rear shield	-3.01	-7.41	-4.4	18.1
Deck	3.79	-3.71	-7.5	30.9
Front	0.09	0.08	0.0	0.1
Bonnet	0.37	0.49	0.1	-0.5
Base	5.91	2.02	-3.9	16.0
Overall	-106.01	-130.29	-24.3	100

8 Mechanism of aerodynamic damping

To look into the mechanism of how the models produce the opposite aerodynamic damping characteristics, particularly at the trunk deck, we performed a detailed flow analysis above the trunk deck regions. Figure 8 shows the phase-averaged aerodynamic lift exerted on the trunk deck. During tail-up pitching cycle, L_{deck} progressively decreases in model B, which indicates that the resulted M tended to resist the vehicle's pitching motion - stabilizing. In model A however, L_{deck} increases in the latter half of the cycle. Hence, the resulted M is destabilizing. During tail-down pitching cycle, the progressively increasing trend in model B again implies a stabilizing tendency. While model A exhibits a destabilizing tendency in the earlier half of the cycle.

Figure 9 shows the static pressure difference Δp in trunk deck between each quadrant of pitching cycle. First, let us examine the causes for the destabilizing influence by aerodynamics in model A. From φ = 90 to 180°, the L_{deck} decreases due to the decreases of static pressure in the central region (marked I). The cross flow velocity vectors in Figure 10 depicts that there are stronger circulatory structures in the central region of trunk deck at φ = 180°. This is due to two factors. First, the strength of A-pillar vortex has increased with pitch angle, as may be evidenced by the higher C_{ptot} core. Second, at maximum pitch angle, the clearance between the stronger A-pillar vortex and trunk deck becomes smaller. Hence, relatively stronger cross flows are generated in the clearance. These cross flows which approach from both sides form an upwash structures as they converged at the centerline. This observation agrees with the results obtained with sedan-type simple bodies by Cheng et al (2011 and 2012).

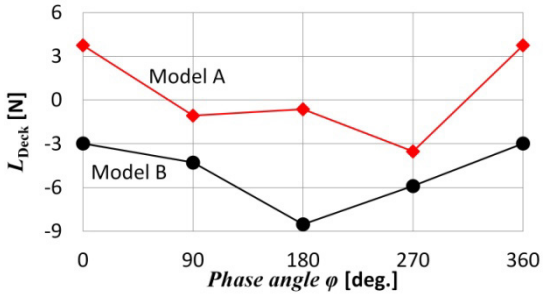

Figure 8: Phase-averaged L on deck: (a) Model A and (b) Model B.

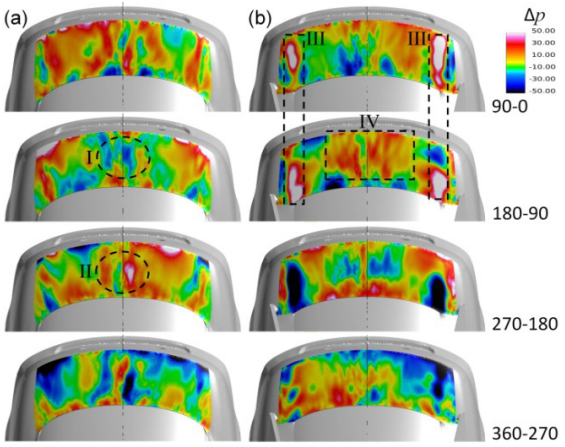

Figure 9: Trunk deck Δp: (a) Model A and (b) Model B.

From φ = 180 to 270°, the destabilizing tendency is caused by the rise of static pressure in the central region (marked II). At φ = 270°, the trunk deck surface is farther away from the A-pillar vortex. This could be the reason why the upwash structures decreases and results in a higher static pressure on the trunk deck.

Now, let us examine the causes for the stabilizing influence of aerodynamics in model B. During tail-up pitching cycle, the increases of static pressure at the sides of trunk deck (mark III) is due to the attenuation

of C-pillar vortex with pitch angle. At larger pitch angle, the slant angle of C-pillar decreases. Hence, it generates a weaker longitudinal vortex with lower induced pressure drop.

At each side of trunk deck, the C-pillar vortex rotates in direction that draws the airflow towards the centerline. As such, the surface pressure in the central region increases (marked IV) when the weakening C-pillar vortex induces lesser cross flow at higher pitch angle. This additional pressure increment might be the reason for the steeper drop in L_{deck} from $\varphi = 180$ to 270°. During tail-down pitching cycle, the opposite tendency occurs. First, the vortex induced pressure at the sides decreases as the C-pillar vortex becomes stronger. Second, the surface pressure in the central region decreases.

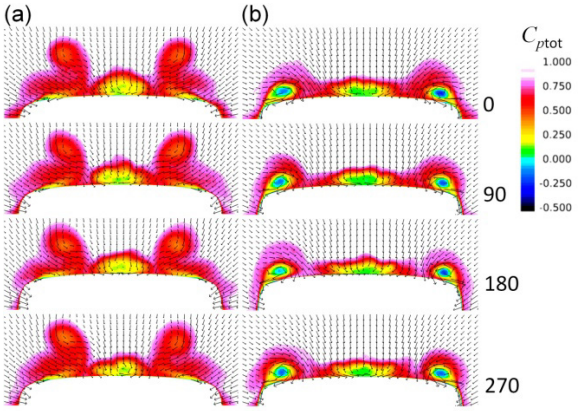

Figure 10: Phase-averaged C_{ptot}: (a) Model A and (b) Model B.

9 Conclusions

The present study has introduced a numerical method for assessment of vehicle performance under a transient situation. The results show that the outcomes obtained with sedan-type simple bodies are transferable to the aerodynamics of real vehicle. Hence, the present study has again confirmed that a rounded A-pillar configuration is important for obtaining a stabilizing aerodynamic effect with respect to pitching. With the present numerical method, we are able to improve realism in vehicle aerodynamic simulation by incorporating vehicle body motion, which is inevitable in real life driving situation.

Acknowledgements

This work was supported by the Industrial Technology Research Grant Program in 2007 from the New Energy and Industrial Technology Development Organization (NEDO) of Japan. A portion of this research was also supported by the grant for "Strategic Program—Preliminary Research Field No. 4: Next-Generation Industrial Innovations" from the Ministry of Education, Culture, Sports, Science, and Technology (MEXT)'s "Development and Use of Advanced, High-Performance, General-Purpose Supercomputers Project," and carried out in partnership with the University of Tokyo. This is a cooperative research with Mazda Motor Corporation, and the experimental data provided are greatly acknowledged.

References

Amsden A.A., and Harlow F.H. (1970), A simplified MAC technique for incompressible fluid flow calculations, J Comput Phys, 6, pp.322-325

Aschwanden P., Müller J., Knörnschild U. (2006), Experimental study on the influence of model motion on the aerodynamic performance of a race car, SAE Paper 2006-01-0803

Cheng S.Y., Tsubokura M., Nakashima T., Nouzawa T., Okada Y. (2011), A numerical analysis of transient flow past road vehicles subjected to pitching oscillation. J. Wind Eng. Ind. Aerodyn, 99, 511-522

Cheng S.Y., Tsubokura M., Nakashima T., Okada Y., Nouzawa T. (2012), Numerical quantification of aerodynamic damping on pitching of vehicle-inspired bluff body, J. Fluid Struct, 30, pp. 188-204

Kim J., and Moin P. (1985), Application of a fractional step method to incompressible Navier-Stokes equations, J Comput Phys, 59, pp.308-323

Hirt C.W., Amsden A.A. and Cook J.L. (1974), An Arbitrary Lagrangian-Eulerian Computing Method for All Flow Speeds, J Comput Phys, 14, pp. 227-253

Howell J. and Le Good G. (1999), The Influence of Aerodynamic Lift on High Speed Stability, SAE Technical Paper 1999-01-0651

Muzaferija S. (1994), Adaptive finite volume method for flow predictions using unstructured meshes and multigrid approach, Ph.D thesis, Univ. of London

Okada Y., Nouzawa T., Nakamura T., and Okamoto S. (2009), Flow structures above the trunk deck of sedan-type vehicles and their influence on high-speed vehicle stability, 1st report: On-road and wind-tunnel studies on unsteady flow characteristics that stabilize vehicle behavior, SAE Int. J. of Passenger Cars – Mechanical Systems, 2(1), pp.138-156, 2009

van Leer B. (1977) Toward the ultimate conservative difference scheme 4, a new approach to numerical convection, J Comput Phys, 23, pp.276-99

Rhie C.M., and Chow W.L. (1983), A numerical study of the turbulent flow past an isolated airfoil with trailing edge separation, AIAA Journal, 21, pp.1525-32

Tsubokura M., Kitoh K., Oshima N., Nakashima T., Zhang H., Onishi K., and Kobayashi T. (2007), Large Eddy Simulation of Unsteady Flow around a Formula Car on Earth Simulator, SAE 2007 Trans. J. of Passenger Cars –Mechanical Systems, 2007-01-0106

Tsubokura M., Nakashima T., Kitoh K., Sasaki Y., Oshima N., and Kobayashi T. (2009), Development of an Unsteady Aerodynamic Simulator Using Large-Eddy Simulation Based on High-Performance Computing Technique, SAE Int. J. of passenger Cars – Mechanical Systems, 2(1), pp.168-178